Computers and Structures 87 (2009) 167–176

Contents lists available at ScienceDirect

Computers and Structures

journal homepage: www.elsevier.com/locate/compstruc

Efficient finite element modelling of reinforced concrete beams retrofitted with fibre reinforced polymers

M. Barbato *

Department of Civil and Environmental Engineering, Louisiana State University, 3531 Patrick F. Taylor Hall, Baton Rouge, LA 70803, USA

ARTICLE INFO

Article history:
Received 7 July 2008
Accepted 19 November 2008
Available online 4 January 2009

Keywords:
Nonlinear finite element analysis
Reinforced concrete structures
Fibre reinforced polymers
Bonding
Strengthening

ABSTRACT

This paper presents a new simple and efficient two-dimensional frame finite element (FE) able to accurately estimate the load-carrying capacity of reinforced concrete (RC) beams flexurally strengthened with externally bonded fibre reinforced polymer (FRP) strips and plates. The proposed FE, denoted as FRP–FB-beam, considers distributed plasticity with layer-discretization of the cross-sections in the context of a force-based (FB) formulation. The FRP–FB-beam element is able to model collapse due to concrete crushing, reinforcing steel yielding, FRP rupture and FRP debonding.

The FRP–FB-beam is used to predict the load-carrying capacity and the applied load-midspan deflection response of RC beams subjected to three- and four-point bending loading. Numerical simulations and experimental measurements are compared based on numerous tests available in the literature and published by different authors. The numerically simulated responses agree remarkably well with the corresponding experimental results. The major features of this frame FE are its simplicity, computational efficiency and weak requirements in terms of FE mesh refinement. These useful features are obtained together with accuracy in the response simulation comparable to more complex, advanced and computationally expensive FEs. Thus, the FRP–FB-beam is suitable for efficient and accurate modelling and analysis of flexural strengthening of RC frame structures with externally bonded FRP sheets/plates and for practical use in design-oriented parametric studies.

1. Introduction

Retrofit of reinforced concrete (RC) members using externally bonded fibre reinforced polymer (FRP) components has become a very common practice, widely recognized by modern design codes [1–5]. In particular, the flexural strength of a beam can be significantly increased by application of carbon (CFRP) or glass (GFRP) FRP plates/sheets adhesively bonded to the beam tension face. This paper focuses on efficient and accurate finite element (FE) modelling of RC beams flexurally retrofitted with externally bonded FRP plates/sheets.

FRP-retrofit of RC beams for flexural strengthening presents numerous advantages compared to other flexural strengthening techniques, e.g., strengthening using steel plates. Some of these advantages are: small increase in structural size and weight, easy transportation, speed and simplicity of in situ application, and good resistance to corrosion and other degradation processes due to hostile environmental conditions. This technique has found numerous applications in retrofitting of bridges and buildings during the last two decades. At the same time, extensive experimental, analytical and numerical research has been carried out to understand and model the structural behaviour of FRP-strengthened RC beams. For literature reviews on different aspects of FRP-strengthening of RC structures, the interested reader is referred to [6–10]. Particular attention has been given to recognizing and understanding the failure modes that RC beams retrofitted with FRP can experience. The experimentally identified failure modes can be grouped as follows: (1) flexural failure by concrete crushing or by steel yielding followed by concrete crushing (flexure failure mode, which is similar to the failure mode of conventional/non-retrofitted RC beams), (2) flexural failure due to FRP rupture (FRP rupture failure mode), (3) flexural failure due to plate end interfacial debonding, to concrete cover separation or to intermediate crack induced debonding (debonding failure mode), and (4) shear failure. A more detailed description of these failure modes can be found in [6]. It is noteworthy that all the failure modes typical of FRP-retrofitted beams (i.e., FRP rupture and debonding) are brittle in nature. In addition, the debonding failure modes correspond to a less than optimal use of the strength capabilities of the FRP material. In order to increase the efficiency of the FRP-retrofit reducing the impact of debonding failure modes, mechanical anchorage techniques have been devised and employed, e.g., use of mechanical devices at the FRP plate/sheet ends, FRP sheets wrapped around the RC member at the FRP plate/sheet ends (U-wrap), and U-shaped FRP plates/sheets along the entire length of the RC beam (U-shape) [11].

* Tel.: +1 225 578 8719; fax: +1 225 578 4945.
E-mail address: mbarbato@lsu.edu

0045-7949/$ - see front matter © 2008 Elsevier Ltd. All rights reserved.
doi:10.1016/j.compstruc.2008.11.006

In the existing literature, numerous studies deal with modelling of FRP-strengthened RC members for bending behaviour and correlation of experimental results with numerically predicted ultimate flexural strength, e.g., [11–23]. Understanding and modelling of debonding failure modes has been and still is a very active field of research, mainly due to the complexity of the problem at hand. Indeed, there is a strong need of reliable and robust formulations of specialized FEs that could help researchers to model accurately FRP-strengthened RC members and structures in order to predict their response under different strengthening configurations, e.g., for design-oriented parametric studies.

Previous FE studies of FRP-retrofitted beams involve the use of refined FE meshes of (1) frame elements with an increased number of DOFs per element when compared to a classical Euler–Bernoulli frame element [24], (2) two-dimensional plate/shell elements [25–28], or (3) three-dimensional solid elements [29]. The high computational cost of structural response analyses based on FE models such as the ones referred above has prompted the development of purely numerical methods (i.e., not based on mechanics) for the analysis and design of FRP-strengthened RC structures [30]. The research work presented in this paper develops a new nonlinear frame FE, based on the classical Euler–Bernoulli assumptions, and able to model the mechanical behaviour of FRP-strengthened RC beams. This FE, referred to as FRP–FB-beam in the sequel, (1) allows reducing the complexity and computational cost of FE analyses based on existing FE models, (2) provides a sound mechanical description and interpretation of the phenomena leading to failure of FRP-retrofitted RC beams, and (3) simulates the structural response of the considered structural systems with accuracy satisfactory for practical applications.

2. Finite element modelling

2.1. Finite element formulation

A two-node frame FE able to model RC structural members retrofitted with externally bonded FRP strips/plated is developed using a force-based formulation (see [31–34]) with Euler–Bernoulli kinematic assumptions. Linear geometry is also assumed (small deformations and small displacements). A two-dimensional fibre-discretization (i.e., a layer-discretization) is employed to describe the cross-section nonlinear behaviour [31–33]. Realistic nonlinear constitutive models are employed to represent the stress–strain behaviour of concrete, reinforcing steel and bonded FRP. Element state determination is performed following a Gauss–Lobatto integration scheme with a user-defined number of integration points (cross-sections).

It is noteworthy that the computational efficiency of the proposed frame element stems from the use of the force-based formulation. For frame elements, the force-based formulation relies on force interpolation functions that strictly satisfy the equilibrium of bending moments and axial force at any point along the element [31]. Thus, force-based frame elements are exact within the framework of the classical beam theories. The FE models built by using force-based frame elements are virtually mesh-independent, in the sense that the same mesh discretization can be used for linear and nonlinear FE analysis without loss of accuracy. The accuracy of the proposed element derives from the capability of the fibre-section model of predicting the nonlinear flexural behaviour at the cross-section level.

2.2. Computation of cross-section stress resultants

The cross-section stress resultants (bending moment and axial force) are computed using a fibre (layer) discretization of the cross-section [31–33] (see Fig. 1). The stress–strain behaviour of each layer is described through a one-dimensional nonlinear constitutive model for the corresponding material. The FRP reinforcement is modelled as additional fibres positioned at the bottom and top of the concrete cross-section. Notice that, for beams, the FRP strip/plate is usually positioned only on the tension side of the structural element. The response of the FRP reinforcement is computed assuming that the slip between FRP and concrete surface is negligible (i.e., conservation of the planarity of cross-sections is assumed). Due to the above simplifying assumption, the bond-slip relation at the FRP–concrete interface is not directly modelled in the FE developed in this study. Instead, the bond-slip behaviour is accounted for indirectly, since an appropriate bond-slip model is used to determine the maximum force that can be carried by the FRP reinforcement. This maximum force is then used to define the parameters required to fully characterize the FRP reinforcement constitutive model. A possible extension of the proposed FRP–FB-beam FE is the explicit modelling of the slip at the FRP–concrete interface, similarly to the FE proposed in [24].

In this paper, realistic one-dimensional nonlinear constitutive models are employed to describe the stress–strain behaviour of each of the layers in which the cross-sections are discretized. The selected constitutive law for the concrete material is a uniaxial cyclic law with a monotonic envelope given by the Popovics–Saenz law [35–37]. A typical cyclic response of the concrete material model adopted herein is shown in Fig. 2. The behaviour in tension

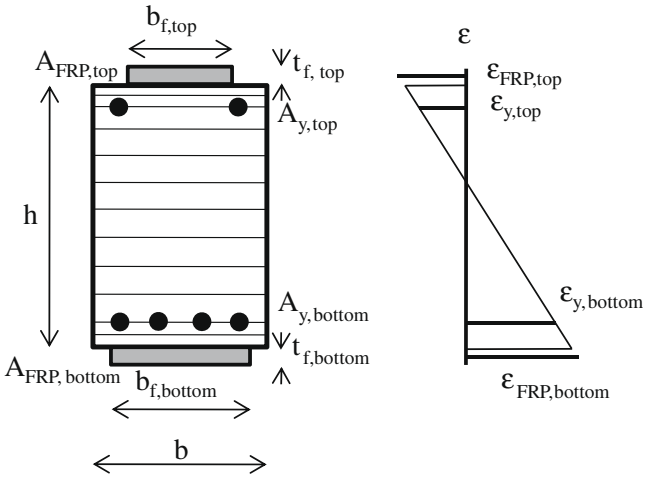

Fig. 1. Generic cross-section geometry, layer-discretization and strain distribution under the hypothesis of conservation of section planarity.

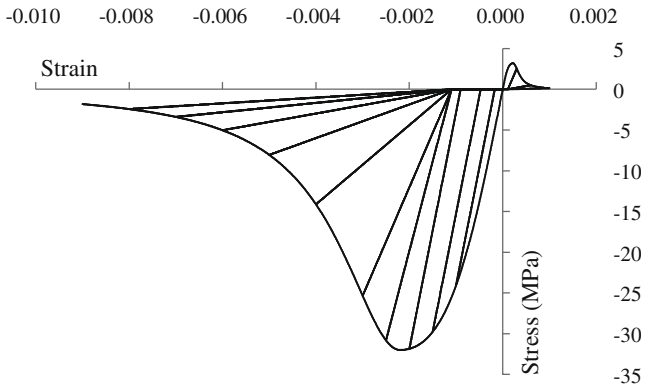

Fig. 2. Hysteretic Popovics–Saenz concrete material model: typical cyclic stress–strain response.

is obtained scaling down (by a user-defined scaling factor) the concrete compressive behaviour, keeping as a constant the initial tangent stiffness at zero strain. A more detailed description of this constitutive model can be found in [38,39].

The reinforcing steel is modelled by using the one-dimensional Menegotto–Pinto (M–P) plasticity model [40]. This plasticity model is a computationally efficient smooth inelastic model typically used for structural steel, showing very good agreement with experimental results, particularly from cyclic tests on reinforcing steel bars. Furthermore, the M–P model can accommodate modifications to account for local buckling of steel bars in RC members [41], and has been extended for efficient and accurate FE response sensitivity computation [42]. A typical cyclic response of the steel material model adopted herein is shown in Fig. 3.

The FRP reinforcement is modelled with elastic-brittle behaviour in tension and zero-strength and stiffness in compression. The failure strain in tension is obtained as the minimum between the material rupture strain and the debonding strain, computed using an appropriate debonding model. The FRP contribution to the element strength and stiffness is accounted for through the usual hypothesis of section planarity. This allows considering FRP plates/sheets in analogy with a reinforcement positioned at the tension side of the section, whose contribution is automatically accounted for within the fibre-section state determination.

The proposed FE is able to model cyclic and dynamic response of RC beams retrofitted with externally bonded FRP plates/sheets. The current implementation does not model strength and stiffness degradation due to repeated cycles of hysteresis, which is beyond the scope of this paper. However, this limitation can be eliminated simply by implementing in the FE code material constitutive models including strength and stiffness degradation due to repeated cycles of hysteresis.

2.3. FRP constitutive model including debonding

Debonding is a common failure mode in FRP plates/sheets strengthening of RC elements in flexure. In the literature, many semi-empirical models exist that describe and evaluate debonding stresses of FRP plates/sheets externally bonded to a concrete surface [9]. In this work, the Monti–Renzelli model for debonding is employed (see [43–45]). This model is described by the following two equations yielding the maximum stress that the FRP sheet can carry before debonding, σ_d, and the corresponding effective bonded length L_e, which is defined as the anchorage length beyond which no increase in the carried FRP stress is obtained:

$$\sigma_d = \beta \cdot \sqrt{\frac{E_f \cdot \tau_{\max}}{c_0 \cdot t_f}} \tag{1}$$

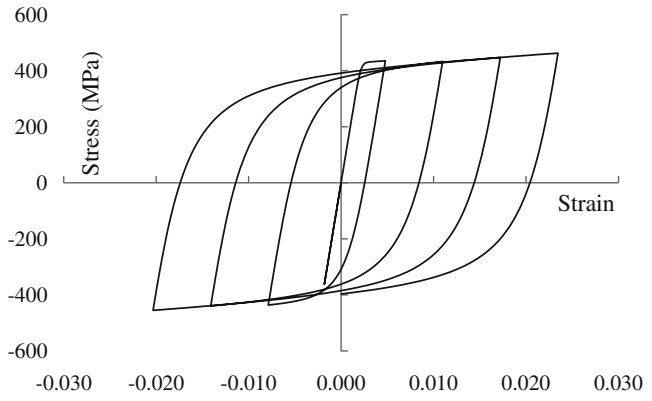

Fig. 3. Menegotto–Pinto material constitutive model for structural steel: typical cyclic stress–strain response.

$$L_e = \sqrt{\frac{E_f \cdot t_f}{\sqrt{c_1} \cdot \tau_{\max}}} \tag{2}$$

where

$$\beta = \begin{cases} 1 & L \geqslant L_e \\ \sin\left(\frac{\pi L}{2L_e}\right) & L < L_e \end{cases}$$

L = actual FRP anchorage length, E_f = FRP elastic modulus, t_f = thickness of the FRP reinforcement, $\tau_{\max}$ = peak bond stress, obtained as

$$\tau_{\max} = k_b \cdot 1.8 \cdot f_{\text{ctm}} \tag{3}$$

in which f_{ctm} = concrete mean tensile strength, k_b = parameter accounting for scale effects, given by

$$k_b = \sqrt{\frac{1.5 \cdot (2 \cdot b_f / b_c)}{1 + b_f / b_{\text{ref}}}} \tag{4}$$

with b_f = width of FRP plate/sheet, and b_c = width of concrete surface. The constants c_0 in Eq. (1), c_1 in Eq. (2) and b_{ref} in Eq. (4) have been obtained in [43] through parametric studies using finite element analysis in conjunction with experiments and have the following values: $c_0 = 3\ \text{mm}^{-1}$, $c_1 = 4\ \text{MPa mm}^{-2}$, and $b_{\text{ref}} = 100$ mm. Eqs. (1)–(4) assume as units of measure MPa (for σ_d, E_f, $\tau_{\max}$, and f_{ctm}) and mm (for L_e, t_f, b_f, and b_c). The Monti–Renzelli model is suitable to describe debonding of FRP strips/plates on uncracked concrete and linear anchorage. When mechanical anchorage is provided, the maximum stress at debonding, σ_d, is modified to account for the anchorage mechanism. In this study, σ_d is assumed (1) equal to the maximum between the value obtained from Eq. (1) with $\beta = 1$ (i.e., $L \geqslant L_e$) and the stress at rupture of the FRP material, σ_r, in correspondence of cross-sections where a mechanical anchorage device is located (e.g., bolts, complete or partial wrapping of the section reinforced flexurally with FRP), and (2) equal to the minimum of σ_d obtained from Eq. (1) with $\beta = 1$ and σ_r in all other cross-sections for members with mechanical anchorage at the ends of the reinforcing strip/plate. Three anchorage types have been modelled in this study: (1) use of bolts at the end of the FRP reinforcement, (2) partial wrapping (or U-wrap) at the end of the FRP reinforcement, and (3) use of wings or of strips/plates shaped so to cover also the sides of the beam along its entire length (U-shape). In particular, U-wrap is a procedure very common in practical applications to ensure anchorage of FRP reinforcement. The effects of the U-wrap and U-shape anchorage are modelled indirectly as previously described, neglecting the contribution to the load-carrying capacity of the RC members due to the FRP material positioned along the sides of the retrofitted structural member.

The FRP constitutive law used to describe the stress–strain behaviour of the corresponding layer at each integration point is elastic-brittle in tension. Stiffness and strength in compression are assumed equal to zero. Two independent parameters are needed to fully describe the constitutive model of the FRP material accounting for debonding, namely E_f and $\sigma_f = \min(\sigma_r, \sigma_d)$ = FRP failure stress. Possible prestressing can be included in the model by introducing an initial deformation given as: $\varepsilon_{f0} = F_{pr}/(t_f \cdot b_f \cdot E_f)$, where F_{pr} = prestressing force.

The adopted constitutive law for the FRP is given by (see Fig. 4):

$$\sigma = \begin{cases} E_f \cdot (\varepsilon + \varepsilon_{f0}) & \varepsilon_{\max} \leqslant \sigma_f / E_f - \varepsilon_{f0} \quad \text{and} \quad \varepsilon > -\varepsilon_{f0} \\ 0 & \text{otherwise} \end{cases} \tag{5}$$

in which σ = current stress, ε = current strain, $\varepsilon_{\max}$ = maximum value of ε over the entire time-history analysis. Eq. (5) describes a linear elastic behaviour for strains $-\varepsilon_{f0} < \varepsilon < \sigma_f / E_f - \varepsilon_{f0}$ conditional to the fact that $\varepsilon_{\max} \leqslant \sigma_f / E_f - \varepsilon_{f0}$. It is also assumed that the bonding between FRP and concrete is not damaged if the FRP plate/sheet experiences compression strains. In order to model the brittle

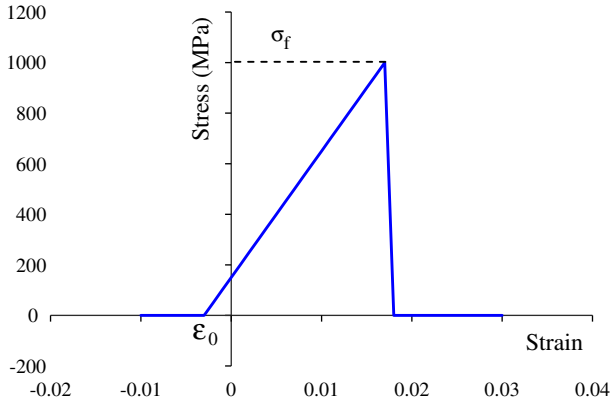

Fig. 4. FRP material constitutive model including debonding and prestressing.

nature of structural collapse due to FRP rupture and/or debonding, when the FRP reaches failure in one of the cross-sections of a specific FE, it is assumed that the FRP reaches failure also in all other cross-sections of the same FE.

2.4. Computer implementation

The above formulation for nonlinear FE response analysis of RC members flexurally strengthened with externally bonded FRP strips/plates was implemented in FEDEASLab [46], a Matlab [47] toolbox suitable for linear and nonlinear, static and dynamic structural analysis.

Taking advantage of the modularity of FEDEASLab, the existing element, section, and material libraries were extended (i.e., 6-DOF displacement-based RC beam element with FRP flexural reinforcement, 6-DOF force-based RC beam element with FRP flexural reinforcement: FRP–FB-beam element, cross-section with FRP reinforcement including debonding, new cyclic FRP material model including debonding) to enable accurate modelling and response simulation of RC structures with members flexurally strengthened with externally bonded FRP sheets/plates. These FE libraries can be easily updated and/or extended to reflect the state-of-the-art in modelling such structures (e.g., including more advanced models for debonding and introducing FEs accounting for slip between FRP reinforcement and concrete). In particular, the development of a nonlinear frame element able to model shear retrofit using FRP strips/plates and column confinement using FRP is currently under study.

3. Correlation between numerical simulation and experimental results

An extensive correlation study between experimental results and numerical simulations has been carried out as part of the research presented in this paper. Fifty eight different configurations of RC beams have been included in the experimental database: 13 sets of tests on reference RC beams without FRP reinforcement and 45 sets of tests on RC beams flexurally retrofitted using externally bonded FRP strips/plates. The corresponding experimental data are available in the literature and have been collected from 11 different authors [11,14–23]. Most of the considered experimental results are presented in terms of ultimate load-carrying capacity of simply-supported FRP-retrofitted RC beams subjected to a 4-point bending test (Fig. 5a). The results presented in [22] were obtained from 3-point bending tests (Fig. 5b).

Several authors have successfully attempted and presented comparisons of load-carrying capacity of FRP-retrofitted RC beams measured from experimental tests and estimated through FE analysis. Previous FE studies of FRP-retrofitted beams involved the use of refined FE meshes of frame elements, two-dimensional plate/shell elements, or even three-dimensional solid elements. The newly developed frame FE presented here allows reducing the complexity and computational cost associated with existing FE models and, at the same time, reaching a level of accuracy which is satisfactory for practical applications. In fact, the results presented in this study are obtained through nonlinear incremental FE analysis of very simple models characterized by extremely coarse meshes. These FE models exploit the symmetry of the structure and the applied loading, and are constituted by only two FEs for 4-point bending tests and only one FE for 3-point bending tests (Fig. 6).

The nonlinear FE analyses are performed using an incremental displacement-controlled technique based on a Newton–Raphson iterative procedure [48] in which the vertical displacement is applied at the loading points and the internal resisting force is computed. This numerical procedure is intended to reproduce the experimental procedure used when also post-peak behaviour is of interest. It is noteworthy that the use of force-based frame elements eliminates possible numerical difficulties in connection with softening and strength loss of individual cross-sections [32]. Five Gauss–Lobatto integration points are employed along each frame element constituting the FE model. Anchorage lengths are obtained from the geometry of the FRP reinforcement.

3.1. Prediction of ultimate load-carrying capacity

The performance of the newly developed frame FE is evaluated through a comparison between the experimentally measured and the numerically predicted load-carrying capacity of the beams included in the experimental database. Table 1 provides the geometric properties of the specimens and the most important mechanical properties of the used materials, including both reference (i.e., non-retrofitted) and FRP-retrofitted beams. Geometric properties of the specimens and mechanical properties of the materials are taken from the test data and available experimental information provided in the referred literature [11,14–23] and mostly obtained through steel coupon and FRP tensile tests or concrete compression tests. In some of the considered references, the properties of the

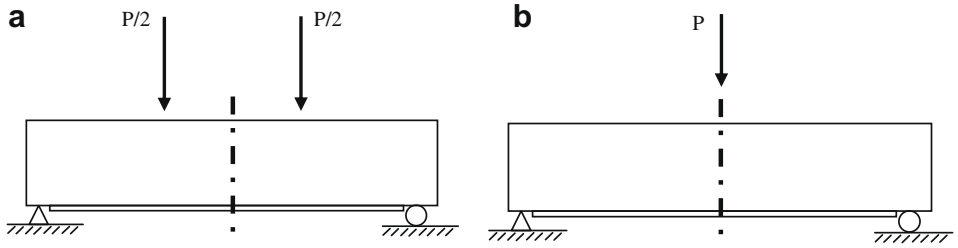

Fig. 5. Experimental setup: (a) 4-point bending tests, and (b) 3-point bending tests.

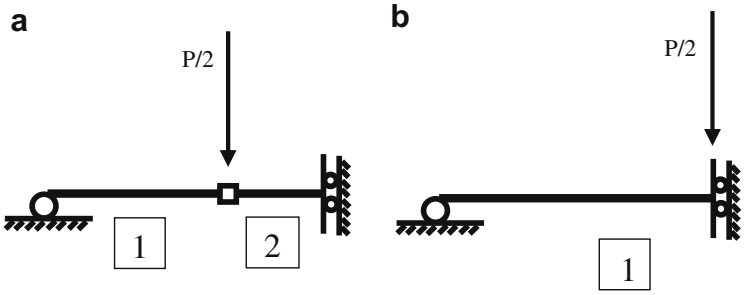

Fig. 6. FE mesh: (a) 4-point bending tests, and (b) 3-point bending tests.

Table 1
Experimental test database: geometry and material properties of RC beam specimens (a superscript "3-point" identifies specimens subjected to 3-point bending test).

Authors	ID	Shear span (mm)	Width (mm)	Height (mm)	$A_{y,bottom}$ (mm^2)	$A_{y,top}$ (mm^2)	f_c (MPa)	f_y (MPa)	E_y (GPa)
Ritchie et al. [14]	A	914	152.5	305	265.5	0	43.2	450	202
	B, C, D						40.0		
	E						43.2		
	F						40.0		
	G, H						43.2		
	I						40.0		
	L						40.0		
	M						43.2		
Saadatmanesh and Ehsani [15]	B	1980	205	460	981.7	265.5	35	456	210
Triantafillou and Plevris [16]	A, B, C, D, E, F, G, H, I, L, M	460	76	127	33.2	0	44.7	517	200
Sharif et al. [11]	1, 2, 3, 4, 5, 6, 7, 8	393	150	150	157.1	56.5	37.7	450	210
Al Soulaimani et al. [17]	JO, JP	400	150	150	339.3	56.5	37.7	450	200
Zarnic et al. [18]	Slab	960	800	120	384	256	25	460	210
	Beam		200	300	340	226			
Wu and Niu [19]	RC1–RC2	900	150	200	402.1	265.5	30.2	360	210
	RCS1						34.6		
Ahmed et al. [20]	AF.0, AF.2, AF.2-1, AF.3, AF.4	500	125	225	100.5	56.5	41.0	568	185
	CF.3-0				150.7	56.5	43.0		
	DF.1, DF.2						42.0		
	DF.4						40.5		
Almusallam and Al-Salloum [21]	F0, FG1, FG2, FG4, FC1, FC2	925	150	200	235.6	28.3	37.5	415	200
Eng [22]$^{3\text{-point}}$	5	1016	203	305	402.1	402.1	49.8	428.6	190
	20		305	305	603.2		41.3		
Maalej and Leong [23]	A1, A2, A3, A4, A5, A6	500	115	146	235.6	235.6	42.8	547	180
	B1, B2, B3, B4, B5, B6	1000	230	292	942.5	942.5		544	183
	C1, C2, C3, C4, C5	1600	368	467.2	2412.7	2412.7	42.4	552	181

FRP materials were provided directly by the producers. Results corresponding to beams experiencing shear failure have been excluded in the present correlation study, since the FRP–FB-beam element does not model shear failure. The considered database contains specimens with a wide range of shear span lengths (from 393 mm to 1980 mm), cross-section widths (from 76 mm to 800 mm), cross-section heights (from 120 mm to 467.2 mm), steel reinforcement areas (from 33.2 mm^2 to 2412.7 mm^2 in the tension side and from 0 mm^2 to 2412.7 mm^2 in the compression side) and concrete peak strength (from 25 MPa to 49.8 MPa). It is noteworthy that the beam specimens are quite small compared with beams currently used in actual buildings, with the only exception of the specimens B in [15] and C1 through C5 in [23]. In particular, the study presented in [23] focuses on beam size effects for FRP-retrofitted beams. Table 2 provides the geometric and mechanical properties of the FRP reinforcement and the corresponding anchorage systems. The experimental database used in this study includes a wide variety of FRP reinforcement configurations, with two materials (CFRP and GFRP), FRP stiffness from 11.7 GPa to 270 GPa, and four different anchorage systems, i.e., (1) linear anchorage, in which the anchorage is provided only by the bonding between FRP and concrete through the adhesive layer, (2) U-wrap, in which an FRP sheet is bonded at each plate end from one side to the other of the beam cross-section, (3) Bolts + U-wrap, in which bolts are positioned at each FRP plate end in addition to the U-shaped FRP sheet, and (4) U-shape, in which the FRP plate/sheet is bonded also on the sides of the RC beam cross-section along the entire length of the FRP reinforcement.

Table 3 shows the comparison between experimental results and numerical simulations of the load-carrying capacities of the reference RC beams. In this case, the proposed FRP–FB-beam element reduces to a conventional distributed plasticity FB frame element. The agreement between load-carrying capacities experimentally obtained and numerically simulated is excellent: the mean of the ratio between FE simulations and corresponding experimental results, $R = P_{FE}/P_{exp}$, is $\mu_R = 1.03$ and its coefficient

Table 2
Experimental test database: geometry and material properties of FRP reinforcement for FRP-retrofitted RC beams (a superscript "3-point" identifies specimens subjected to 3-point bending test).

Authors	ID	Material	t_f (mm)	b_f (mm)	E_f (GPa)	ε_r (%)	Anchorage
[14]	C–D	GFRP	4.76	152.5	11.7	1.37	Linear
	E						U-wrap
	F		9.52				Linear
	G		4.19		10.35	1.78	
	H		9.26		20.69	1.17	
	I		4.06		27.6	1.16	
	L	CFRP	1.27		54.47	1.12	
	M				117.9	1.13	
[15]	B	GFRP	6	152	37.2	1.07	Linear
[16]	2	CFRP	0.2	42.6	186	0.78	Linear
	3			60.5			
	4–5		0.65	63.2			
	6–7		0.9	63.3			
	8		1.9	63.9			
[11]	P1	GFRP	1	100	15	1.15	Linear
	P2		2				
	P3		3				
	P2BW		2				Bolts + U-wrap
	P3BW		3				
	P3J		3				U-wrap
[17]	JP	GFRP	3	100	16	1.25	U-wrap
[18]	Slab 1, 2, 3	CFRP	1.2	100	150	1.6	Linear
	Beam 1, 2, 3		1.2	50			
[19]	RC1–RC2	CFRP	0.11	140	230	1.39	Linear
	RCS1		0.22				
[20]	AF.2	CFRP	0.334	75	240	1.46	Linear
	AF.2-1						
	AF.3						
	AF.4						
	DF.1		0.167				
	DF.2		0.334				
	DF.4		0.668				
[21]	FG1	GFRP	1.3	150	27.58	2	U-shape
	FG2		2.6				
	FG4		5.2				
	FC1		1		68.95	1.5	
	FC2		2				
[22]$^{3\text{-point}}$	5	GFRP	3.21	102	61.6	1.43	Linear
	20						
[23]	A3–A4	CFRP	0.165	107.8	235	1.51	Linear
	A5–A6		0.33				
	B3–B4		0.33	215.6			
	B5–B6		0.66				
	C3–C4		0.495	368			
	C5		0.99				

Table 3
Comparison between experimental results and numerical simulation of load-carrying capacity of reference RC beams (i.e., without FRP retrofit).

Authors	ID	$(P/2)_{exp}$ (kN)	$(P/2)_{FE}$ (kN)	P_{FE}/P_{exp}	Failure mode
[14]	A	36.5	38.49	1.05	Flexure
[16]	A	36.5	38.49	1.05	Flexure
	B	36.2	37.71	1.04	Flexure
[11]	CB	26.5	26.44	1.00	Flexure
[17]	JO	50.1	48.34	0.96	Flexure
[18]	Slab 0	33.5	33.36	0.99	Flexure
	Beam 0	80.0	80.02	1.00	Flexure
[20]	AF.0	27.5	27.89	1.01	Flexure
	CF.3-0	37.5	41.75	1.11	Flexure
[21]	F0	17.65	17.77	1.01	Flexure
[23]	A1–A2	30.28	31.85	1.05	Flexure
	B1–B2	101.05	109.12	1.08	Flexure
	C1–C2	259.78	276.20	1.06	Flexure
All (13 cases)	Mean = **1.03**	St. Dev. = **0.04**	COV = **0.04**	Min. = **0.96**	Max. = **1.11**

of variation (COV) is COV = 0.04. The maximum and minimum values of R are 1.11 and 0.96, respectively. All beams failed in flexure, with yielding of the steel in tension preceding concrete crushing in compression.

Table 4 provides the experimentally measured and numerically simulated values of the load-carrying capacities of the FRP-retrofitted RC beams, the ratio R and the corresponding failure mode. The simulation capabilities of the proposed FRP–FB-beam element are very good, with $\mu_R = 0.97$ and COV = 0.13. The maximum and minimum values of R are 1.39 and 0.68, respectively, showing a larger scatter compared to the FE simulations for conventional unstrengthened RC beams.

Another very important feature of the FRP–FB-beam element is that it provides the failure mode experienced by the structural model in addition to the numerical response. The failure modes found in the FE simulations for each specimen agree with the failure modes reported in the research studies included in the experimental database. The most common failure mode is the debonding failure mode (31 cases): the FRP–FB-beam element is able to recognize the location of the initiation of debonding, i.e., if debonding starts at the plate end or at the location of maximum moment. The FRP–FB-beam element does not provide information to distinguish between plate end interfacial debonding and concrete cover separation and models in the same way debonding of the FRP plate/sheet on both uncracked and cracked concrete. A possible future improvement of the proposed FE could be the use of the model presented in [43] to differentiate the intermediate crack induced debonding of FRP plates/sheets from debonding in uncracked concrete zones. Even with these limitations, the FE prediction capabilities of load-carrying capacity for beams failing due to debonding

Table 4
Comparison between experimental results and numerical simulation of load-carrying capacity of FRP-retrofitted RC beams (a superscript "3-point" identifies specimens subjected to 3-point bending test).

Authors	ID	$(P/2)_{exp}$ (kN)	$(P/2)_{FE}$ (kN)	P_{FE}/P_{exp}	Failure mode
[14]	C–D	57.5	57.57	1.00	Debonding
	E	62.3	69.16	1.11	Debonding
	F	66.5	72.50	1.09	Debonding
	G	62.9	55.07	0.88	Debonding
	H	55.7	77.27	1.39	Debonding
	I	50.6	67.22	1.33	Debonding
	L	61.4	60.80	0.99	FRP rupture
	M	72	74.40	1.03	Debonding
[15]	B	124	115.38	0.93	Debonding
[16]	2	6.6	7.65	1.16	FRP rupture
	3	8.6	8.96	1.04	FRP rupture
	4–5	13.8	13.65	0.99	Debonding
	6–7	14.6	15.31	1.05	Debonding
	8	18.7	19.07	1.02	Debonding
[11]	P1	33.5	27.66	0.83	FRP rupture
	P2	34	30.17	0.89	Debonding
	P3	33	31.84	0.96	Debonding
	P2BW	39	33.22	0.85	Flexure
	P3BW	36	38.66	1.07	Flexure
	P3J	41	38.66	0.94	Flexure
[17]	JP	62.3	59.81	0.96	Flexure
[18]	Slab 1–2–3	30.65	27.24	0.89	Debonding
	Beam 1–2–3	57.83	56.04	0.97	Debonding
[19]	RC1–RC2	33.5	30.57	0.91	Debonding
	RCS1	36.8	35.16	0.96	Debonding
[20]	AF.2	41.5	37.88	0.91	Debonding
	AF.2-1	42.85	37.88	0.88	Debonding
	AF.3	48.25	37.88	0.79	Debonding
	AF.4	55.5	37.95	0.68	Debonding
	DF.1	59	44.82	0.76	FRP rupture
	DF.2	60	48.44	0.81	Debonding
	DF.4	62.5	53.05	0.85	Debonding
[21]	FG1	35.2	35.22	1.00	Flexure
	FG2	41.2	41.66	1.01	Flexure
	FG4	52.95	50.90	0.96	Flexure
	FC1	40.95	41.42	1.01	Flexure
	FC2	51.55	48.55	0.94	Flexure
[22]$^{3\text{-point}}$	5	72.5	73.03	1.01	Debonding
	20	93	96.24	1.03	Debonding
[23]	A3–A4	38.25	37.30	0.98	Debonding
	A5–A6	43.3	41.78	0.96	Debonding
	B3–B4	130.95	137.85	1.05	Debonding
	B5-B6	144.75	137.77	0.95	Debonding
	C3-C4	330.55	338.38	1.02	Debonding
	C5	325.05	311.20	0.96	Debonding
All (45)	Mean = **0.97**	St. Dev. = **0.13**	COV = **0.13**	Min. = **0.68**	Max. = **1.39**
Debonding (31)	Mean = **0.98**	St. Dev. = **0.14**	COV = **0.14**	Min. = **0.68**	Max. = **1.39**
Flexure (9)	Mean = **0.97**	St. Dev. = **0.06**	COV = **0.06**	Min. = **0.85**	Max. = **1.07**
FRP rupture (5)	Mean = **0.96**	St. Dev. = **0.16**	COV = **0.17**	Min. = **0.76**	Max. = **1.16**

are remarkably good, with $\mu_R = 0.98$ and COV = 0.14. The second most common failure mode is the flexure failure mode with 9 cases. For this failure mode, the prediction capabilities of the FRP–FB-beam element are excellent and comparable with the ones obtained for unstrengthened RC beams, with $\mu_R = 0.97$ and COV = 0.06. Finally, five cases of FRP rupture failure modes are also recorded experimentally and identified by the FE simulations, with $\mu_R = 0.96$ and COV = 0.17. The data seem to show that FE simulations for FRP-retrofitted RC beams are slightly less accurate and present a slightly larger dispersion than FE results corresponding to other failure modes.

Fig. 7 graphically reproduces the results shown in Tables 3 and 4. The dashed line on the main diagonal corresponds to perfect agreement between experimental results and numerical simulations, i.e., $R = 1.00$. The results are grouped and identified by different symbols based on the experienced failure mode. Fig. 7 shows also that most of the tests refer to beams with load-carrying capacity lower than 100 kN. Nevertheless, the results corresponding to the few larger beams included in the considered experimental database suggest that the accuracy of the proposed FRP–FB-beam element in predicting the load-carrying capacity of FRP-retrofitted beams is not affected by scale effects.

Notice that, in Tables 3 and 4 and Fig. 7, the results from different specimens with identical geometric and mechanical properties are averaged and the obtained mean values are considered in evaluating the accuracy of the FRP–FB-beam element.

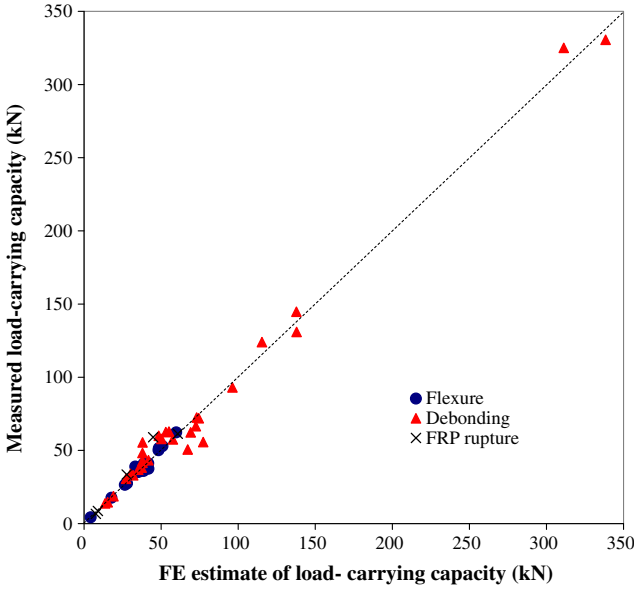

Fig. 7. Comparison between experimental measurement and FE simulation of the maximum applied force (ultimate load-carrying capacity).

3.2. Comparison of load-deflection response

This study carried out also a comparison between experimentally recorded and numerically simulated applied load-midspan deflection response of reference and FRP-retrofitted beams. Only few of the database studies contain also the applied load-midspan deflection responses of the tested specimens. Here, the results corresponding to the study presented in [18] are shown and described in detail. The geometric properties of the specimens, tested in 4-point bending, are shown in Fig. 8.

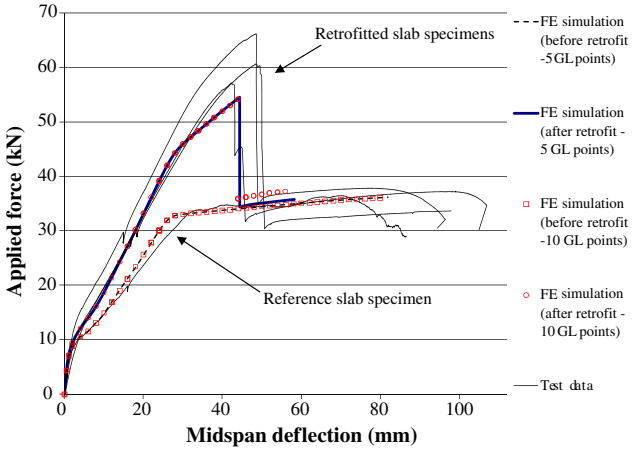

Fig. 9. Comparison between experimental measurement and FE simulation of the applied force-midspan deflection response for the slab specimens for the tests presented in [18].

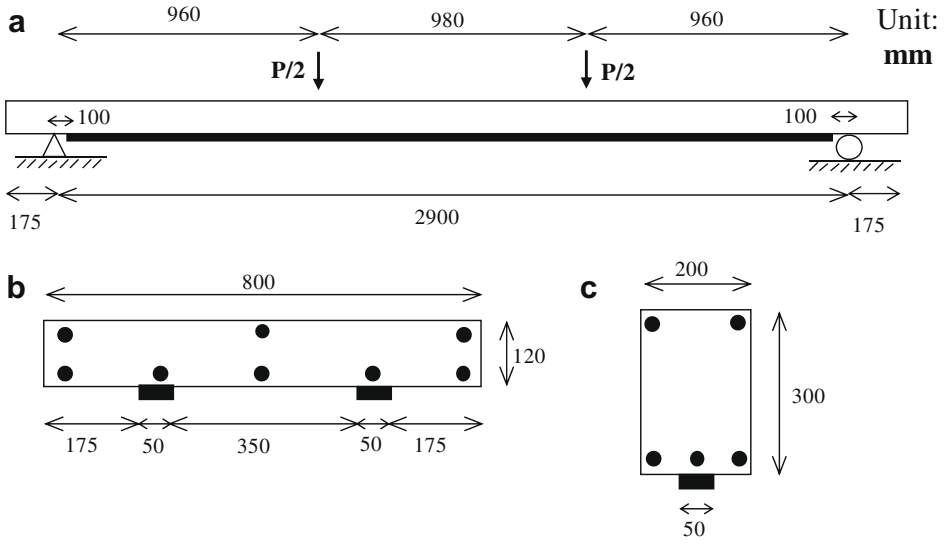

Fig. 8. Geometric properties of the specimens tested in [18]: (a) shear span and loading condition for both slab and beam specimens, (b) cross-section geometry of the slab specimens, and (c) cross-section geometry of the beam specimens.

Fig. 9 plots the applied load-midspan deflection responses for the reference slab specimen and the three equally-built FRP-retrofitted slab specimens. The thin solid lines correspond to the recorded experimental results; the two thick solid lines represent the FE response simulations for FE meshes built with two FEs with five Gauss–Lobatto (GL) integration points each; the markers (squares for the reference beam and circles for the FRP-retrofitted beams) provide the FE response simulation for FE meshes built with two FEs with 10 GL integration points each. The agreement between numerical simulations and experimental records is excellent for the reference slab and very good for the FRP-retrofitted slabs. In addition, it is observed that results from the two FE meshes with five and 10 GL integration points are almost coincident, confirming that the use of five GL integration points is sufficient to ensure objectivity of the results before the peak strength is reached.

The FE simulation slightly underestimates the flexural strength and the ductility of the FRP-retrofitted slabs, but captures extremely well their initial stiffness, stiffness after cracking of the concrete in tension and post-peak stiffness. On the other hand, the estimate of the ductility after yielding of the steel in tension has not been attempted, since the proposed FRP–FB-beam element does not include any method to ensure objectivity of the modelling of softening structural behaviour (see [49]).

For this specific case, precise modelling of the configuration of the FRP reinforcement, which is bonded to the beam soffit as two separate sheets (see Fig. 8b), is crucial for accurate simulation of the structural response. In fact, the results presented herein are obtained computing the parameter k_b in Eq. (4) from the geometric properties of a single FRP sheet applied to half of the slab cross-section, i.e., using $b_f = 50$ mm, and $b_c = 400$ mm. With these values for the parameters b_f and b_c, the slab load-carrying capacity obtained from FE simulation is $P_{FE} = 54.48$ kN and is reached for a midspan deflection $\delta = 44.4$ mm. If the particular configuration of the FRP reinforcement is not taken correctly into account (i.e., if the previous parameters are taken as $b_f = 100$ mm, and $b_c = 800$ mm), the FE simulation yields $P_{FE} = 50.47$ kN (7.3% reduction in predicted strength) and $\delta = 37.4$ mm (15.8% reduction in predicted midspan deflection).

Fig. 10 plots the applied load-midspan deflection responses for the reference beam specimen and the three equally-built FRP-retrofitted beam specimens. Similarly to Fig. 9, the thin solid lines correspond to the recorded experimental results; the two thick solid lines represent the FE response simulations for FE meshes with two FEs employing five GL integration points per element; the markers provide the FE response simulation for FE meshes with two FEs employing 10 GL integration points each. Also in this case, the agreement between numerical simulations and experimental records is excellent for the reference beam and very good for the FRP-retrofitted beam. In particular, the ratio between the numerical prediction and the experimental measure of the load-carrying capacity for the FRP-retrofitted beams is $R = 0.97$. In addition and similarly to the previous case, the FE results from the two FE meshes with five and 10 GL integration points are almost coincident, confirming that, also for the beam specimens, the use of five GL integration points is sufficient to ensure objectivity of the results before the peak strength is reached. The midspan deflection at peak strength and the applied force at which the concrete starts cracking in tension are slightly underestimated, while the post-peak stiffness is slightly overestimated. It is noteworthy that the differences between the experimental responses for the three retrofitted beams are much smaller than in the case of the retrofitted slabs. In addition, the response of this specific beam model has been found very sensitive to the value of the concrete strength in tension (see also [24]), which is a parameter difficult to estimate accurately.

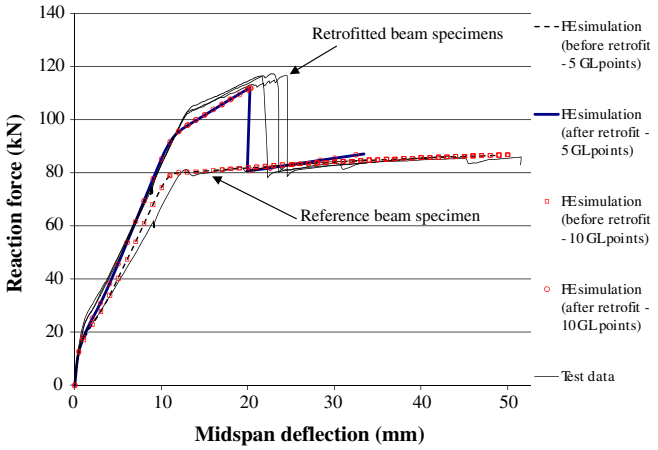

Fig. 10. Comparison between experimental measurement and FE simulation of the applied force-midspan deflection response for the beam specimens for the tests presented in [18].

The results presented show that the proposed FRP–FB-beam element is able to predict accurately the load-carrying capacity of FRP-retrofitted beams, the corresponding failure mode and the applied load-midspan deflection response. The accuracy of the proposed FE depends also on the ratio R_S between shear span and cross-section height and degrades for decreasing R_S. In particular for $R_S < 3$, the shear behaviour has, in general, a significant effect on both beam strength and deformation. The proposed FE is not able to model shear failure and shear deformation. If the shear failure is prevented by adequate shear reinforcement, the proposed FRP–FB-beam element may predict the FRP-retrofitted beam strength with accuracy sufficient for practical applications, but would produce inaccurate predictions of the midspan deflections, since it neglects linear and nonlinear shear deformations.

4. Conclusions

This paper presents a simple and efficient two-dimensional frame FE, denoted as FRP–FB-beam, able to accurately simulate the response of RC beams flexurally strengthened with externally bonded FRP strips and/or plates. The FRP–FB-beam is developed from a force-based formulation and considers distributed plasticity with layer-discretization of the cross-sections. The FRP–FB-beam is able to model different failure modes experimentally observed, i.e., collapse due to concrete crushing, reinforcing steel yielding, FRP rupture, FRP debonding at the plate ends and intermediate crack induced debonding. The FE proposed can also model different anchorage systems devised to increase the force carried by the FRP plate/sheet before debonding takes place.

The presented FE is used to predict the ultimate load-carrying capacity of beams subjected to three- and four-point bending loading. Numerical simulations and experimental measurements are compared based on numerous tests available in the literature and published by different authors. The agreement between experimental results and numerical simulations is very good. In addition, the FE results, obtained employing very coarse meshes built using the FRP–FB-beam element, provide information on the specific failure mode experienced by the considered structural system. Recorded and simulated applied load-midspan deflection responses are also compared, showing again a very good agreement.

The major features of this frame FE are its simplicity and its efficiency in terms of mesh refinement. The FE is developed and implemented so that interaction between axial and bending behaviour is automatically accounted for through the cross-section

discretization in layers. In addition, all nonlinear material constitutive models are developed and fully implemented to accommodate cyclic quasi-static and dynamic analysis. Thus, this FE is suitable for modelling and analyzing flexural strengthening of RC frame structures using FRP plates and/or sheets and to perform efficiently and accurately parametric studies on different retrofitting configurations. Extension of the proposed FRP–FB-beam FE to FRP-retrofit of shear strength deficient frame members is currently under study.

Acknowledgements

The author gratefully acknowledges partial support of this research by the Louisiana Board of Regents through the Pilot Funding for New Research (Pfund) Program of the National Science Foundation (NSF) Experimental Program to Stimulate Competitive Research (EPSCoR) under Award No. NSF (2008)-PFUND-86. Opinions expressed in this paper are those of the author and do not necessarily reflect those of the sponsor. The author would also like to acknowledge Professor G. Monti of the University of Rome "La Sapienza" (Italy) for his invaluable guidance at the beginning of the author's research on FRP-strengthened RC structures.

References

[1] JSCE, Recommendations for upgrading of concrete structures with use of continuous fiber sheets. Technical Report, Research Committee on Upgrading of Concrete Structures with Use of Continuous Fiber Sheets, Japanese Society of Civil Engineers; 2000.
[2] Fib Bullettin 14, Externally bonded FRP reinforcement for RC structures. Technical Report, Federation Internationale du Beton; 2001.
[3] ISIS, Retrofitting concrete structures with fiber reinforced polymers. ISIS, Canada; 2001.
[4] ACI 440, Guide for the design and construction of externally bonded FRP systems for strengthening concrete structures. Technical Report, American Concrete Institute; 2002.
[5] CS 55, Design guidance for strengthening concrete structures using fibre composite materials. Technical Report, Concrete Society, UK; 2004.
[6] Smith ST, Teng JG. FRP-strengthened RC beams I: review of debonding strength. Eng Struct 2002;24:385–95.
[7] Teng JG, Chen JF, Smith ST, Lam L. FRP-strengthened RC structures. West Sussex: Wiley; 2002.
[8] Teng JG, Chen JF, Smith ST, Lam L. Behaviour and strength of FRP-strengthened RC structures: a state-of-the-art review. Proc Inst Civil Eng, Struct Build 2003;156(1):51–62.
[9] Karbhari VM, Niu H, Sikorsky C. Review and comparison of fracture mechanics-based bond strength models for FRP-strengthened structures. J Reinf Plast Compos 2006;25:1757–94.
[10] ACI 440R-07, Report on fiber-reinforced polymer (FRP) reinforcement for concrete structures. Technical Report 440, American Concrete Institute; 2007.
[11] Sharif A, Al-Sulaimani GJ, Basunbul IA, Baluch MH, Ghaleb BN. Strengthening of initially loaded reinforced concrete beams using FRP plates. Struct J (ACI) 1994;91(2):160–8.
[12] Van Gemert D. Force transfer in epoxy-bonded steel-concrete joints. Int J Adhes Adhes 1980;1:67–72.
[13] An W, Saadatmanesh H, Ehsani MR. RC beams strengthened with GFRP plates. II: analysis and parametric study. J Struct Eng (ASCE) 1991;117(11):3434–55.
[14] Ritchie A, Thomas DA, Lu LW, Connelly GM. External reinforcement of concrete beams using fiber reinforced plastics. Struct J (ACI) 1991;88(4):490–500.
[15] Saadatmanesh H, Ehsani MR. RC beams strengthened with GFRP plates. I: experimental study. J Struct Eng (ASCE) 1991;117(11):3417–33.
[16] Triantafillou TC, Plevris N. Strengthening of RC beams with epoxy bonded fiber composite materials. Mater Struct 1992;25:201–11.
[17] Al-Sulaimani GJ, Sharif A, Basunbul IA, Baluch MH, Ghaleb BN. Shear repair for reinforced concrete by fiberglass plate bonding. Struct J (ACI) 1994;91(3):458–64.
[18] Zarnic R, Gostic S, Bosiljkov V, Bokan-Bosiljkov V. Improvement of bending load-bearing capacity by externally bonded plates. In: Dhir RK, Henderson NA, editors. Proceedings creating with concrete. London: Thomas Telford; 1999. p. 433–42.
[19] Wu ZS, Niu HD. Study on debonding failure load of RC beams strengthened with FRP sheets. J Struct Eng (JSCE) 2000;46(A):1431–41.
[20] Ahmed O, Van Gemert D, Vandewalle L. Improved model for plate-end shear of CFRP strengthened RC beams. Cement Concrete Compos 2001;23:3–19.
[21] Almusallam TH, Al-Salloum YA. Ultimate strength prediction for RC beams externally strengthened by composite materials. Compos: Part B 2001;32:609–19.
[22] Eng C. The use of mechanical anchorage in FRP strengthening of reinforced concrete beams. Master Thesis, Department of Structural Engineering. CA, USA, University of California San Diego; 2004.
[23] Maalej M, Leong KS. Effect of beam size and FRP thickness on interfacial shear stress concentration and failure mode of FRP-strengthened beams. Compos Sci Technol 2005;65(7–8):1148–58.
[24] Aprile A, Spacone E, Limkatanyu S. Role of bond in RC beams strengthened with steel and FRP plates. J Struct Eng (ASCE) 2001;127(12):1445–52.
[25] Jerome DM, Ross CA. Simulation of the dynamic response of concrete beams externally reinforced with carbon-fiber reinforced plastic. Comput Struct 1997;64(5-6):1129–53.
[26] Rahimi H, Hutchinson A. Concrete beams strengthened with externally bonded FRP plates. J Compos Constr (ASCE) 2001;5(1):44–56.
[27] Moller B, Graf W, Hoffmann A, Steinigen F. Numerical simulation of RC structures with textile reinforcement. Comput Struct 2005;83:1659–88.
[28] Camata G, Spacone E, Zarnic R. Experimental and nonlinear finite element studies of RC beams strengthened with FRP plates. Compos Part B 2007;38:277–88.
[29] Kotynia R, Baky HA, Neale KW, Ebead UA. Flexural strengthening of RC beams with externally bonded CFRP systems: test results and 3D nonlinear FE analysis. J Compos Constr (ASCE) 2008;12(2):190–201.
[30] Flood I, Muszynski L, Nandy S. Rapid analysis of externally reinforced concrete beams using neural networks. Comput Struct 2001;79:1553–9.
[31] Spacone E, Filippou FC, Taucer FF. Fiber beam-column element for seismic response analysis of reinforced concrete structures. UCB/EERC Rep. 91/17, Earthquake Engineering Research Center, University of California, Berkeley, Richmond, CA, USA; 1991.
[32] Spacone E, Filippou FC, Taucer FF. Fibre beam-column element for nonlinear analysis of R/C frames. Part I: formulation. Earthquake Eng Struct Dyn 1996;25:711–25.
[33] Spacone E, Filippou FC, Taucer FF. Fibre beam-column element for nonlinear analysis of R/C frames Part II: application. Earthquake Eng Struct Dyn 1996;25:727–42.
[34] Neuenhofer A, Filippou FC. Evaluation of nonlinear frame finite-element models. J Struct Eng (ASCE) 1997;123(7):958–66.
[35] Balan TA, Filippou FC, Popov EP. Constitutive model for 3D cyclic analysis of concrete structures. J Eng Mech (ASCE) 1997;123(2):143–53.
[36] Balan TA, Spacone E, Kwon M. A 3D hypoplastic model for cyclic analysis of concrete structures. Eng Struct 2001;23:333–42.
[37] Kwon M, Spacone E. Three-dimensional finite element analyses of reinforced concrete columns. Comput Struct 2002;80:199–212.
[38] Zona A, Barbato M, Conte JP. Finite element response sensitivity analysis of steel-concrete composite structures. Technical Report SSRP-04/02, Department of Structural Engineering, University of California San Diego, La Jolla, CA, USA; 2004.
[39] Zona A, Barbato M, Conte JP. Finite element response sensitivity analysis of steel-concrete composite beams with deformable shear connection. J Eng Mech (ASCE) 2005;131(11):1126–39.
[40] Menegotto M, Pinto PE. Method of analysis for cyclically loaded reinforced concrete plane frames including changes in geometry and nonelastic behavior of elements under combined normal force and bending. In: Proceedings, IABSE symposium on resistance and ultimate deformability of structures acted on by well-defined repeated loads, Zurich, Switzerland; 1973. p. 112–23.
[41] Monti G, Nuti C. Nonlinear cyclic behavior of reinforcing bars including buckling. J Struct Eng (ASCE) 1992;118(12):3268–84.
[42] Barbato M, Conte JP. Finite element structural response sensitivity and reliability analyses using smooth versus non-smooth material constitutive models. Int J Reliab Safety 2006;1(1–2):3–39.
[43] Monti G, Renzelli M, Luciani P. FRP adhesion to uncracked and cracked concrete zones. In: Proceedings, sixth international symposium on FRP reinforcement for concrete structures (FRPRCS-6), Singapore; 2003.
[44] Monti G, Barbato M. Fiber-section FE of FRP-strengthened RC beam in flexure, shear and confinement. In: Proceedings sixth international symposium on FRP reinforcement for concrete structures (FRPRCS-6), Singapore; 2003.
[45] Barbato M, Monti G, Santinelli F. Fiber-section FE of FRP-strengthened RC beam for seismic analysis. In: Proceedings, fib-symposium concrete structures in seismic regions, Athens, Greece; 2003.
[46] Filippou FC, Constantinides M. FEDEASLab getting started guide and simulation examples. Technical Report NEESgrid-2004-22; 2004. www.neesgrid.org.
[47] MathWorks Inc. Matlab – High performance numeric computation and visualization software. User's guide, Natick, MA, USA; 1997.
[48] Bathe KJ. Finite element procedures. Englewood Cliffs, NJ, USA: Prentice-Hall; 1995.
[49] Coleman J, Spacone E. Localization issues in force-based frame elements. J Struct Eng (ASCE) 2001;127(11):1257–65.